Journal of Ultrafine Grained and Nanostructured Materials
https://jufgnsm.ut.ac.ir
Vol. 52, No.2, December 2019, pp. 175-187
Print ISSN: 2423-6845 Online ISSN: 2423-6837
DOI: 10.22059/jufgnsm.2019.02.06

Improvement of Nanosized CuO-Fe_2O_3/cordierite System by Li_2O-treatment for wastewater treatment; carcinogenic dyes removal, phenol degradation and hydrogen peroxide decomposition

Nouf F. El-Harby[1], Abdelrahman A. Badawy[2,*], Shaimaa M. Ibrahim[3]

[1]Department of Chemistry, Faculty of science and arts, Qassim University, Saudi Arabia.
[2]Physical Chemistry Department, National Research Centre, Dokki, Cairo, Egypt.
[3]Department of Chemistry, Faculty of Education, Ain Shams University, Cairo, Egypt.

Recieved: 11 June 2019; Accepted: 30 October 2019
** Corresponding author email: aabadawy107@yahoo.com*

ABSTRACT

A mixture of 10 wt% CuO-10 wt% Fe_2O_3 supported on cordierite were prepared by wet impregnation. The as-prepared solids doped with Li_2O (0.75-3 mol %) were calcined at 500-900 ˚C. The crystalline phase, morphology, and surface area were investigated by XRD, HR-TEM and N_2-adsoprtion-desorption. Moreover, their photocatalytic activities of samples calcined at 700˚C on the degradation of phenol were evaluated under UV-irradiation. The catalytic activity of different solids toward H_2O_2 decomposition was studied. Nano-materials were used to adsorb dyes as Remazole-Red and Congo-Red from aqueous solution. The sorption process was in good agreement of pseudo-second order equation and the Langmuir equation through their adsorption kinetics and isotherms, respectively. The CuO-Fe_2O_3/ cordierite doped with 0.75% Li_2O at 700 ˚C adsorbent was found to possess the highest removal efficiency of Remazole-Red and/or Congo-Red dyes and potentially lowering capital and operational costs for \practical applications. The highest removal efficiency of the anionic dyes over 0.75% Li_2O at 700 ºC can be discussed by observing the appearance of new active phases as CuO, $CuFe_2O_4$ and LiCuO, decreasing the crystallite size of these active phases. 0.75 mol% Li_2O has the greatest activity in H_2O_2 decomposition reached 700 %. This result may be related to the lowest particle size and the highest surface area of this sample, which also produced a large number of electrons donating active sites for H_2O_2 decomposition.

Keywords: *Congo-Red dye, Remazole-Red dye, Copper ferrite, COD, Cordierite, Li_2O- doping, H_2O_2-decomposition*

1. Introduction

A global concern of wastewater from chemical industries and hazardous pollutants present in water supplies [1]. The wastewater from textile processing contains residues [2]. A large amount of organic matter and colorants (dyes) discharge during the textile industry, especially in the coloring and washing steps.

A lot of methods are known for dye removal from wastewater such as precipitation, coagulation and ultra-filtration [3]. These techniques are nondestructive, since they only convert the non biodegradable matter into sludge [3]. In comparison with other techniques, adsorption is the most favorable method in the contaminants removal from wastewater. This probably was used due to its simplest, cost effective and high adsorption capacity for the removal of dyes from wastewater [2,

4]. Considerable researches reported the usage of polymer, activated carbon and fly ash as adsorbent surfaces for dyes adsorption from solutions [5, 6]. The focus of recent researches is the foundation of low cost adsorbents instead of expensive activated carbon in spite of its widespread [7, 8].

However, in recent years, efforts have been made to use mixed oxides nanostructured as an adsorbent for dye removal because of its low cost, large numbers of corner defects sites, unusual lattice planes, high surface area, micro-pore structure and high surface reactivity [9-12], which could greatly facilitate their future adsorption applications. So, the removal of various pollutants could be achieved by using mixed metal oxides that is efficient adsorbent [13-15].

Many reactive azo dyes removal is difficult because of their high solubility in water, complex structure and synthetic origin [16]. Congo- Red (CR) and Remazole-Red (RR) are examples of azo dyes, which are mostly used as dyes in textile industries. They are heavily toxic to the environment. So, removal of these dyes from wastewater has attracted our attention in this study.

Numerous studies utilized Fe_2O_3 as adsorbent for dye removal because of its non-harmfulness, accessibility, high imperviousness to oxidative change and low preparing cost [17, 18]. Adjustment of iron oxide by blending it with different oxides was studied. This was attributed due to its low warm strength, surface territory diminishment and fast deactivation in reactant examinations [17, 18]. CuO/Fe_2O_3 was chosen as potential unstable natural mixes [19]. So, there was a need to modify its characteristics. Cordierite was used in heterogeneous catalysis as it has a great warm resistance and little warm coefficient [20-22]. One of the water quality methods is chemical oxygen demand (COD). COD is viewed as a method of portrayed natural toxins present in wastewater. Measure of natural contaminants and water clean degree can be recognized by COD substance [23-27].

In the present work we studied the factors that may have an impact on the composition, crystalline and surface properties of nano-materials $CuO-Fe_2O_3$/cordierite. The as-prepared adsorbents pure and variously treated Li_2O (0.75 - 3 mol %) were identified by XRD, HR-TEM, and N_2-adsorption/desorption isotherms. Photocatalytic studies of the prepared solids were explored regarding Chemical Oxygen Demand (COD). The removal studies of the Congo-Red and Remazole-Red dyes of pure and variously treated $CuO-Fe_2O_3$/cordierite nanomaterials heated at (500, 700 and 900 °C) have been conducted using batch adsorption experiments. For further illustration the efficiency of doped solids, its catalytic activity toward H_2O_2 decomposition was studied.

2. Experimental

2.1. Materials and catalyst preparation

A given mass of a finely powdered cordierite $Mg_2Al_4Si_5O_{18}$ (commercial grade supplied by Baikowski Inc. company) was impregnated with calculated amounts of a mixture of equal amounts of copper nitrate $[Cu(NO_3)_2.6H_2O]$ and ferric nitrate $[Fe(NO_3)_3.5H_2O]$ dissolved in the least amount of distilled water sufficient to make paste. The pastes were dried at 100 °C then calcined at 500,700 and 900 °C for 4 h. The amounts of copper and ferric nitrates were calculated in a manner that the calcined prepared samples contained 10 wt% CuO and 10 wt% Fe_2O_3. Li_2O-traeted solids (0.75-3 mol%) were prepared by impregnating a known mass of finely powdered support material with different amounts of lithium nitrate solution prior to treating with copper and ferric nitrates followed by drying and calcination at 500,700 and 900 °C for 4 h. The employed chemicals were analytical grade and supplied by Fluka Company.

Congo-Red and Remazole-Red were purchased from DyStarand was used as received without further purification. The UV–visible absorption spectrum of the applied dyes shows characteristic absorption both in UV and visible regions. The concentration of Congo-Red and Remazole-Red was measured throughout the work at λ_{max}= 497 and 520 nm, respectively.

2.2. Techniques

X-ray powder diffractograms of variously solids calcined at 500-900 °C were determined using a Bruker diffractometer (Bruker D 8 advance target). The patterns were run with copper Kα with secondly monochromator (λ = 1.5405 Å) at 40 kV and 40 mA. The scanning rate was 8° and 0.8° in 0.2° in 2θ min^{-1} for phase identification and line broadening profile analysis, respectively. The crystallite size of the phases present in pure and variously supported solids was determined using the Scherrer equation (eq. 1) [28]:

$$d = K \lambda / \beta_{1/2} \cos \theta \qquad \text{(eq. 1)}$$

where d is the mean crystalline diameter, λ is the X-ray wave length, K is the Scherrer constant (0.89), $\beta_{1/2}$ is the full width at half maximum (FWHM) of the main diffraction peaks of the crystalline phase present and θ is the diffraction angle.

The structure and the surface morphology of the resulted nano-materials were examined using JEOL JEM-1230 transmission electron microscope (TEM) with acceleration voltage of about 80 kV and JEOL-SEM scanning electron microscope (SEM), respectively.

The textural properties of the samples were determined by physical adsorbing nitrogen (N_2) at 77K using a Quantachrome Nova-Touch 4LX automated gas-sorption apparatus (USA). Before each N_2- sorption measurement, samples were degassed at -193 ºC for 2 h. The N_2-adsorption on the samples was used to calculate the specific surface area by means of the Brunauer–Emmett–Teller (BET) equation [29]. The pore size distribution was calculated from desorption branch of the isotherm by the Barrett, Joyner and Halenda (BJH) method. Chemical Oxygen Demand (COD) was used to analyze the wastewater before and after the photocatalysis process according to the Standard Methods for Water and Wastewater Examination (APHA, AWWA, 1995) as described in the previous work of one of the author [23-27]. The UV lamp used in order to irradiate samples has a range of wavelengths up to 368 nm.

The amount of catalyst is one of the main parameters for the degradation studies. In order to avoid the use of excess catalyst it is necessary to find out the optimum catalyst loading for efficient removal of COD of the wastewater. Several authors have investigated the reaction rate as a function of catalyst loading in photocatalytic oxidation process [25, 30].

Batch adsorption study of water-soluble reactive dye Remazole-Red or Congo-Red onto CuO-Fe_2O_3/cordierite nanomaterials was carried out in 250 mL beakers which contained 100 mg CuO-Fe_2O_3/cordierite sample and 100 mL dye solution of desired concentration. The solution in the beakers was kept stirred at temperature 25± 0.1 ºC and pH 7. At various time intervals, the solutions were centrifuged at 7000 rpm for 10 min and the absorbance of supernatant solution was recorded by UV–vis spectrophotometer (Shimadzu UV/Vis1601 spectrophotometer, Japan). Langmuir and Freundlich isotherms were used to analyze the adsorption equilibrium [31, 32].

The catalytic decomposition of hydrogen peroxide (H_2O_2) in presence of the CuO-Fe_2O_3/cordierite catalysts was examined by mixing 100 mg of the catalyst with (2 mL H_2O_2+18 mL distilled H_2O) and stirred at room temperature (25 ºC) for 3 h. The volume of oxygen liberated at different time intervals were measured until no further O_2 was liberated and was recalculated under STP. A blank test was done as well simultaneously carried out without catalyst under the same condition.

3. Results and discussion

3.1. XRD investigation of different samples

The X-ray diffractograms of untreated and treated samples with Li_2O (0.75 - 3 mol%) then calcined at 500,700 and 900 ºC were given in Figs. 1-3. These figures reveals: (i) The presence of CuO phase together with copper ferrite ($CuFe_2O_4$) phase (d=2.52Å) (34-0425 JCPDS-ICD). The presence of $CuFe_2O_4$ provided by solid-solid interaction between CuO and Fe_2O_3 that is taken through the following reaction:

$$CuO + Fe_2O_3 \longrightarrow CuFe_2O_4$$

The degree of crystallinity and/or abundance of $CuFe_2O_4$ formed in various solids can be measured by the peak area of the diffraction line at d=2.52Å. The $CuFe_2O_4$ peak area was found to be 13.9, 14.1, 16.2 and 4.9 a.u. for pure, 0.75, 1.5 and 3 mol% Li_2O, respectively. The results might indicate that treatment by Li_2O enhanced the ferrite formation to an extent proportional to Li_2O added till 1.5 mol% Li_2O.

The formation of $CuFe_2O_4$ by the interaction between CuO and Fe_2O_3 in presence of Li_2O might

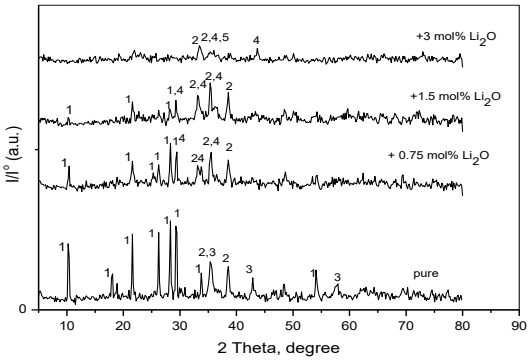

Fig. 1- XRD diffractograms of untreated and treated samples calcined at 500 ºC (1. Cordierite, 2. CuO, 3. Fe_2O_3, 4. $CuFe_2O_4$, 5. Li_2O).

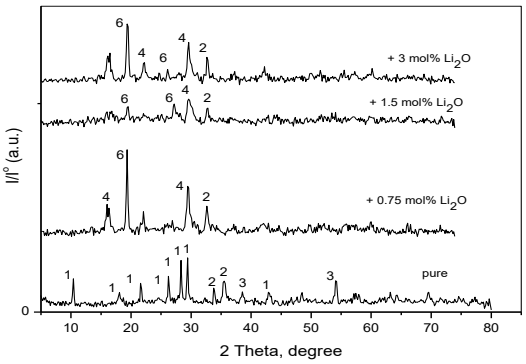

Fig. 2- XRD diffractograms of untreated and treated samples calcined at 700 ºC (1. Cordierite, 2. CuO, 3. Fe_2O_3, 4. $CuFe_2O_4$, 5. Li_2O, 6. LiCuO).

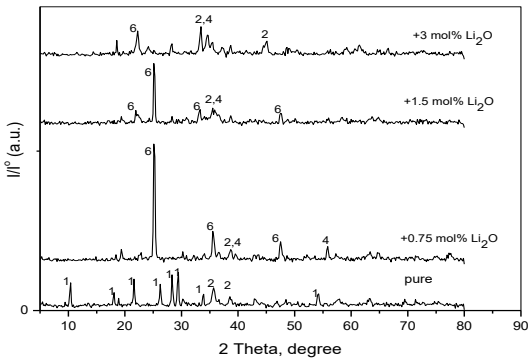

Fig. 3- XRD diffractograms of untreated and treated samples calcined at 900 ºC (1. Cordierite, 2. CuO, 3. Fe_2O_3, 4. $CuFe_2O_4$, 5. Li_2O, 6. LiCuO).

be due to the dissolution of dopant cations (Li^+) in CuO and Fe_2O_3 lattices. The dis-solution process can be discussed by Kröger's notations [33]:

$$2Li^+ + Cu^{2+} \longrightarrow 2Li(Cu^{2+}) + A.V \quad (1)$$

$$Li^+ + Cu^{2+} \longrightarrow Li(Cu^{2+}) + Cu^{2+\delta} \quad (2)$$

$$2Li^+ + Fe^{3+} \longrightarrow 2Li(Fe^{3+}) + C.V \quad (3)$$

where δ is a small portion that increases by increasing the Li^+ dissolved in the treated solids lattice. $Li(Cu^{2+})$ and $Li(Fe^{3+})$ are the monovalent lithium formed in host copper and ferric cations of CuO and Fe_2O_3 lattices, respectively. The substitution process might explain the dissolution. Reactions 1 and 3 showed the presence of anionic and cationic vacancies due to the dissolution of dopant ions in the lattices of reacting oxides. Opposite trends in reaction 2 that showed the decreasing of Cu^{2+} concentration as it is involved in the ferrite formation due to dissolution of lithium ions in lattices. So, applying reaction 1 and 3 showed the stimulation of copper ferrite formation which might be expected up to 1.5 mol%Li_2O. While reaction 2 might exert an opposite effect by addition increasing amounts of Li_2O >1.5 mol%. (ii) New diffraction peaks (d= 3.489Å) of lithium copper oxide (LiCuO) phase (33-0795 JCPDS-ICD) for solids calcined at 700 and 900 °C.This might be expected according to reaction 2 which occurred at high temperature. (iii)The disappearance of cordierite phase for treated samples calcined at 700 and 900 °C might be due to its conversion into amorphous metakaoline [34] and /or presence in small portion that cannot be detected by XRD.

3.2. HR-TEM of various solids

Fig. 4 shows congregate of nano-particles of spherical morphology and relatively uniform with diameter range from 29.48nm to 92.81nm for untreated and for Li_2O supported solids calcined at 700 °C.

3.3. Surface characteristics of different solids

The specific surface area measurements of the selected samples were performed by the BET method from nitrogen adsorption- desorption isotherms obtained at 77K. The outcomes results are shown in Table 1. The results show that: treatment of the supported system investigated calcined at 500 and 700 °C provided a significant increase in the S_{BET} proportional to the amount of lithium oxide present. The maximum increase in the S_{BET} of CuO–Fe_2O_3/cordierite attained 116 %, for solids calcined at 500 °C, treated with 1.5 mol% Li_2O. This significant increase in the S_{BET} values might be due to the decrease in the crystallization of supported material upon treating process with Li_2O (c.f. XRD results). In fact, the surface area increasing due to doping might be accompanied by an improvement in their catalytic activity.

3.4. Photocatalytic degradation of different solids

The photocatalytic degradation of phenol as a model organic pollutant was carried out in presence of the catalysts for different solids calcined at 700 °C under UV irradiation for 120 minutes as shown in Fig. 5. Initially, no phenol degradation activity was observed upon performing the experiment in absence of catalysts or in the dark as be shown in

the previous paper of one of the author [23-27].

Examination of Fig. 5 shows that, the maximum percentage of COD removal for 120 min. reaction was 80%, 94.3%, 84.1% and 82.8% for untreated, 0.75 mol%, 1.5 mol% and 3 mol% Li_2O solids, respectively. The results obtained revealed that Li_2O-treatment was more pronounced than that of CeO_2-doping which has been studied in our pervious paper [25]. This may be related to that Li_2O accelerate the formation of $CuFe_2O_4$ (see XRD section), which is catalytically active constituent [35, 36]. In the present study the

Table 1- specific surface areas (S_{BET}) of different investigated solids calcined at 500, 700 and 900 °C

Solid catalyst	Calcination temperature (°C)	S_{BET}
Cordierite	500	5
CuO – Fe_2O_3/cordierite	500	6.2
CuO –Fe_2O_3/cordierite + 0.75 mol% Li_2O	500	11.4
CuO – Fe_2O_3/cordierite + 1.5 mol% Li_2O	500	12.9
CuO – Fe_2O_3/cordierite + 3 mol% Li_2O	500	8.9
Cordierite	700	4
CuO – Fe_2O_3/cordierite	700	9.4
CuO –Fe_2O_3/cordierite + 0.75 mol% Li_2O	700	13.4
CuO – Fe_2O_3/cordierite + 1.5 mol% Li_2O	700	13.9
CuO – Fe_2O_3/cordierite + 3 mol% Li_2O	700	12
Cordierite	900	4
CuO – Fe_2O_3/cordierite	900	6.2
CuO –Fe_2O_3/cordierite + 0.75 mol% Li_2O	900	6.4
CuO – Fe_2O_3/cordierite + 1.5 mol% Li_2O	900	5.3
CuO – Fe_2O_3/cordierite + 3 mol% Li_2O	900	3.6

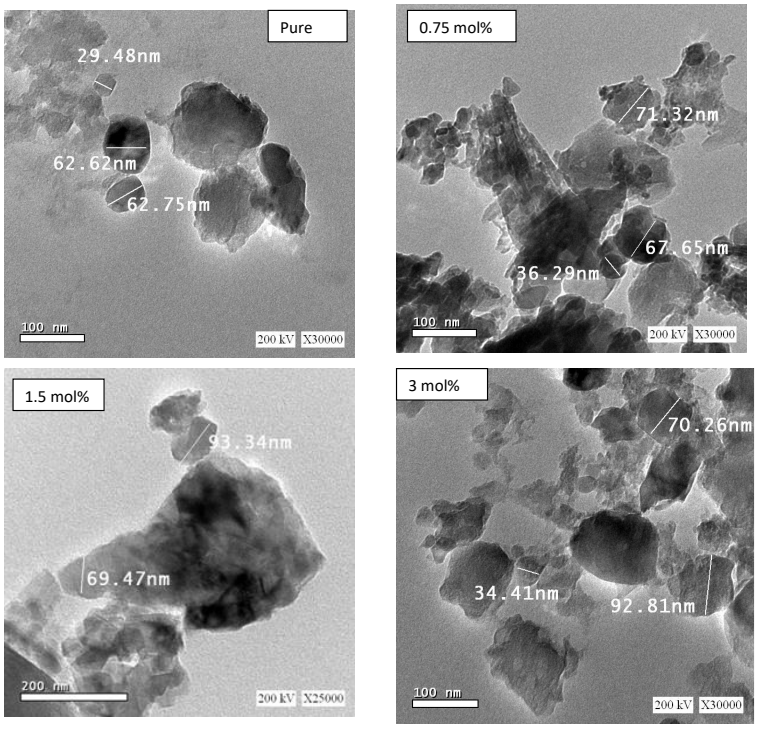

Fig. 4- TEM photographs of untreated and treated samples calcined at 700 ºC.

degradation efficiency was so high, even in absence of H_2O_2 which could be attributed to presence of higher number of surface active sites available for interaction and degradation of phenol. The photocatalytic activity of Li_2O-doped solids refers to the probability of activity toward dye removal.

3.5. Adsorption experiments

3.5.1. Effect of contact time

Adsorption capacity change of different nano-materials towards Remazole-Red or Congo-Red solution with time was depicted in Figs. 6 and 7(a,b). It is clear from these figures that: (i) the adsorption increased gradually and the dye removal percentage improved with time. This might be attributed to vacant adsorption sites on the adsorbent material occupied by dyes deposited [37, 38]. So, the uptake does not change by increasing the contact time more than 160 min. Adsorption rate decreases by time due to the dye molecules occupied the active sites. (ii) It is obvious from Figs. 6 and 7 that the adsorption capacity of the Remazole-Red dye at equilibrium time 200 min. over Pure CuO–Fe_2O_3/cordierite calcined at 500 °C is (3 mg/g) lower than the 0.75% Li_2O doped solid (33 mg/g). This may be due to decreasing the S_{BET} of pure solid which attained 42.5%. Also, increasing the calcination temperature over pure solids led to decreasing the adsorption capacity of Remazole-Red dye. (iii) Fig. 7 b shows that the removal of Congo-Red reaches equilibrium at 160 min on solid doped with 0.75 mol % Li_2O calcined at different calcination temperatures. (iv) The removal efficiency of the Congo-Red dye over 0.75 mol % Li_2O at 700 °C was higher than the doped solids at 500 and 900 °C (amount of dye adsorbed= 27.9 mg/g, removal >80 %) and the complete removal was attained when the contacting time was continued to 200 min. However, decreasing the adsorption capacity and the time of adsorption

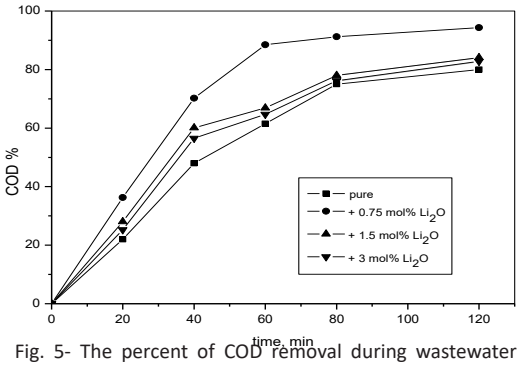

Fig. 5- The percent of COD removal during wastewater treatment by different oxidation processes over different solids calcined at 700 ºC.

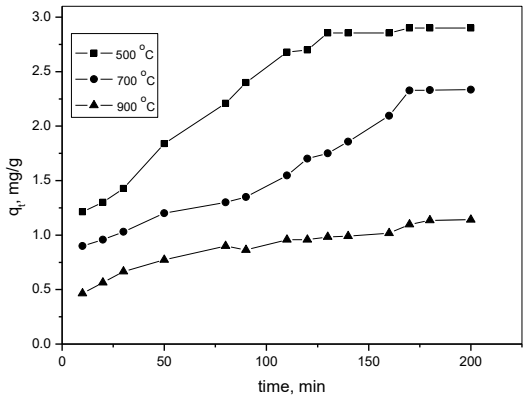

Fig. 6- Effect of contact time on the adsorption capacity of untreated CuO-Fe_2O_3/cordierite calcined at different temperatures toward Remazole-Red dye at 35 ºC (dye concentration = 50 mg L^{-1}).

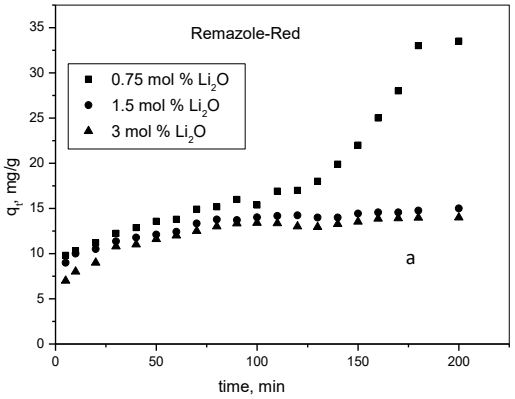

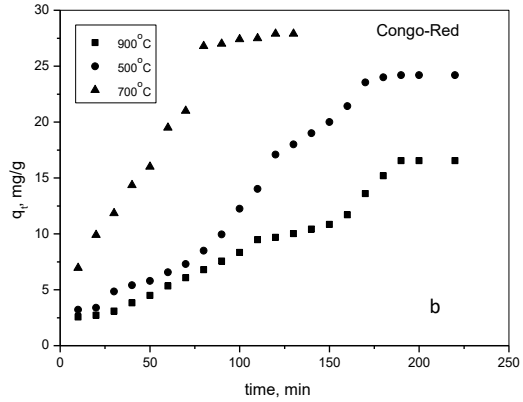

Fig. 7- Effect of contact time on the adsorption capacity of prepared solids calcined at 700 ºC (a) and at different calcination temperatures (b) toward Remazole-Red and Congo-Red dye, respectively at 35 ºC (dye concentration = 50 mg L^{-1}).

of Congo- red dye by increasing the calcination temperature to 900 °C for the 0.75% Li_2O doped solid may be associated with decreasing its surface area (c.f. Table 1). (v) For samples doped with 0.75-3 % Li_2O at 700 °C, the removal efficiency of the Remazole-Red decreased by increasing Li_2O content and maximum adsorption was attained 33 mg/g (95 % removal) when the contacting time was continued to 200 min. Hence, the sample treated with 0.75% Li_2O at 700 °C adsorbent was found to possess the highest removal efficiency of the Remazole-Red dye. The highest removal efficiency of the anionic dyes over 0.75% Li_2O at 700 °C can be discussed by observing the appearance of new active phases as CuO, $CuFe_2O_4$ and LiCuO, decreasing the crystallite size of these active phases (c.f. XRD results), and increasing its S_{BET} higher than the doped samples calcined at 500 and 900 °C.

These results referred that, the doping process of CuO–Fe_2O_3/cordierite system with Li_2O can improve the colloidal efficiency, depending on the chemical adsorption conditions (e.g., contact time), the properties of particles (e.g., S_{BET}), the control of the percentage of Li_2O through preparation step, and the applied calcination temperature for doped solids.

Finally, we can say that the synthesized sample CuO–Fe_2O_3/cordierite doped with 0.75% Li_2O process and calcined at 700 °C was shown to be hopeful adsorbent for the removal of textile dyes from aqueous solutions. This is further emphasized by comparison the adsorption capacity of textile dyes with different adsorbents with the adsorption capacity of the doped solids as shown in Table 2.

3.5.2 .Comparison with other adsorbents

To get an idea about the efficiency of the prepared samples in the dyes adsorption, a Comparison of the highest adsorption capacities of Congo-Red or Remazole-Red dyes over doped CuO-Fe_2O_3/cordierite adsorbent in this work with that of the other previously reported in the literature is shown in Table 2 [39-44]. It shows that the prepared solids in our work possess higher adsorption capacity for Congo-Red and/or Remazole-Red than that of other reported adsorbents which reflects potential utility for the prepared adsorbents utilization in the applied dye removal. In this study, an environmental friendly CuO-Fe_2O_3/cordierite was modified with efficient synthesis of 0.75 mol% Li_2O doping via impregnation method and could efficiently adsorb Congo-Red or Remazole-Red with q_{max} values 34.34, and 33 mg/g, respectively. Results indicated that the synthesized doped samples were shown to be a good adsorbent for the dyes removal from aqueous solutions.

3.5.3. Adsorption isotherms

Langmuir, and Freundlich plots isotherm models on variously prepared nanomaterials calcined at different temperatures were shown in Figs. 8 and 9. The parameters calculated for the two isotherm models were summarized in Tables 3 and 4. Fitting to these equilibrium adsorption data were studied based on the data of the correlation

Table 2- Comparison of the maximum adsorption capacity of different dyes with different adsorbents

No	Adsorbent	Dye	Max. Adsorption capacity (mg/g)	Ref.
1	Hollow Zn-Fe_2O_4 nano-sphere	Congo-Red	16.1	[39]
2	Kaolin (clay materials)	Congo-Red	5.4	[40]
3	Chitosan -GLA	Methyl Orange	7	[41]
4	Chitosan -GLA	Reactive red	7.5	[42]
5	Chitosan -GLA	Congo-Red	24.18	[43]
6	Chitosan -GLA	Indigo carmine	0.613	[44]
7	Chitosan -GLA	Reactive yellow	9	[42]
8	0.75 mol% Li_2O, CuO-Fe_2O_3/cordierite(700 °C)	Congo-Red	34.3	Present study
9	0.75 mol% Li_2O, CuO-Fe_2O_3/cordierite(700 °C)	Remazole-Red	33	Present study
10	Zeolite (clay materials)	Congo-Red	3.8	[40]

coefficient (R^2) of the linear regression plot. Tables 3 and 4 show that the isotherm of Langmuir is good fitting to the adsorption isotherms of Remazole-Red or Congo-Red on different adsorbents with correlation efficient (R^2) higher than 0.99 indicating a good agreement of the data. So, Langmuir model fit to describe the adsorption of Remazole-Red or Congo-Red on different nanomaterials, which confirm the monolayer formation of dye coverage the adsorbent surface. Furthermore, one can find that the constant K_L increase as a following: 0.75 mol% Li_2O > 1.5 mol% Li_2O > 3 mol% Li_2O > un-doped sample. These results revealed that the 0.75 mol% Li_2O nanomaterial has the highest

Table 3- Adsorption isotherm parameters for adsorption of Remazole-Red dye onto variously CuO – Fe2O3 /cordierite doped samples calcined at 500 ºC

sample	Langmuir isotherm model				Freundlich isotherm model		
	q_{max} (mg/g)	K_L (L/mg)	R^2	R_L	K_F (mg/g)	1/n	R^2
0.75mol% Li_2O	24.965	0.01803	0.9895	0.61485	2.42782	1.1557	0.9747
1.5mol% Li_2O	7.9134	0.0144	0.9971	0.7159	1.8729	0.63345	0.9953
3mol% Li_2O	6.4612	0.0114	0.9929	0.67021	2.3128	0.76589	0.9985

Table 4- Adsorption isotherm parameters for adsorption of Congo-Red dye on 0.75mol% Li_2O doped samples calcined at different temperatures.

Calcination temp. (ºC)	Langmuir isotherm model				Freundlich isotherm model		
	q_{max} (mg/g)	K_L (L/mg)	R^2	R_L	K_F (mg/g)	1/n	R^2
500	28.5714	0.038715	0.9927	0.426025	0.248031	1.2384	0.9531
700	34.34221	0.05717	0.9989	0.334502	0.190272	1.819	0.9980
900	8.68809	0.007612	0.9569	0.790578	1.247199	0.6748	0.9277

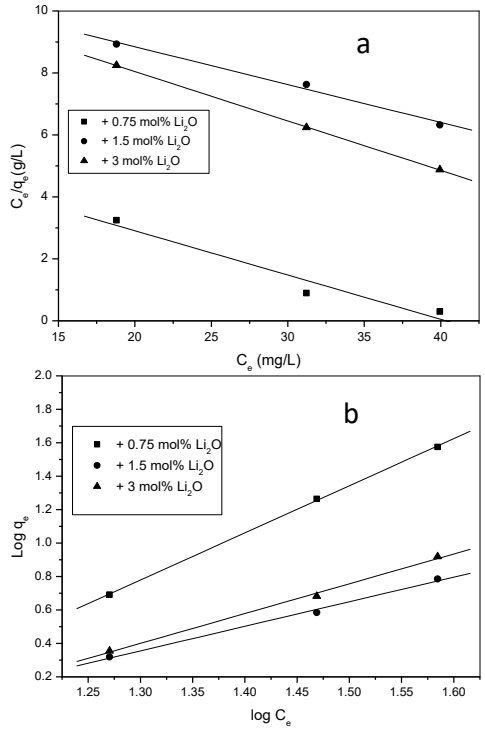

Fig. 8- Langmuir isotherms (A), Freundlich isotherms (B) for Remazole-Red dye adsorption onto variously treated nanomaterials calcined at 500 ºC.

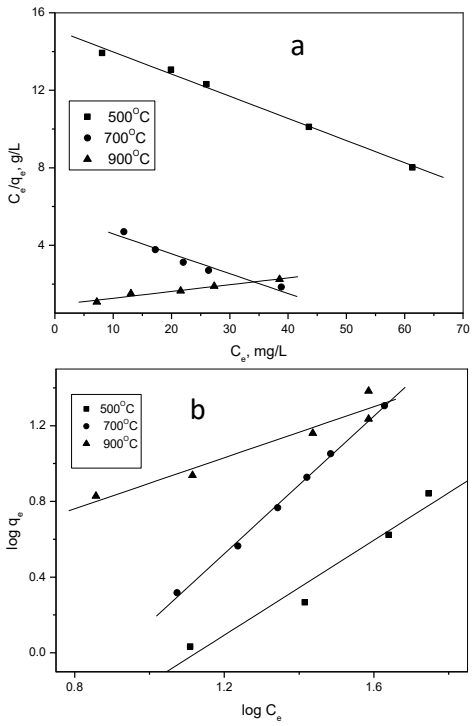

Fig. 9- Langmuir isotherms (a) Freundlich isotherms (b) for Congo-Red dye adsorption onto 0.75mol%Li_2O supported nanomaterials calcined at different temperatures.

adsorption ability. The reason was attributed to its small particle size, highest surface area and pore volume.

The basic component of the isotherm of Langmuir might be described in terms of a dimensionless constant known as separation factor (R_L) [37, 45] studies on which is given by the following equation (eq. 2).

$$R_L = 1/ 1 + K_L C_o \quad \text{(eq. 2)}$$

The R_L values range $0 < R_L < 1$ shows good adsorption [37, 46]. In our study, the range of R_L values 0.334502-0.88456 shows good adsorption of Remazole red or Congo red dyes on different prepared nanomaterials.

3.5.4. Adsorption kinetics

The adsorption plots of Congo-Red and Remazole-Red over 0.75% Li_2O nanomaterials were shown in Figs 10 and 11, respectively. Table 5 shows the data gained for experimental equilibrium adsorption capacity (q_e^{exp}) and calculated equilibrium adsorption capacity (q_e^{cal}) for pseudo first and pseudo second order. The values of k_{dif} were calculated from intra-particle diffusion plot. In addition to the high correlation coefficient values were obtained for pseudo-second-order kinetic models, the q_e data from pseudo-second-order is adjacent to the experimental data better than that calculated from pseudo-first-order kinetic model. So, the adsorption kinetics of Remazole-Red or Congo-Red on different prepared nanomaterials can be described by pseudo- second-order equation.

Fig. 12 represents the plot of q_t versus $t_{0.5}$ for Remazole-Red adsorption by 0.75mol% Li_2O nanomaterials (calcined at 700 ˚C). The experiment data exhibit multi-linear plot. Thus might be discussed by two steps. Phase I; might be due to the immediate utilization of the available sites on the sorbent surface. On other hand, phase II might be due to very slow diffusion of the sorbate from the surface site into the inner pores [37]. So, the ratio of the beginning of Remazole-Red sorption by CuO-Fe_2O_3/cordierite nanomaterials may be showed that surface diffusion process is the rate determing step. The data gained of k_{dif1} and k_{dif2} (diffusion rate

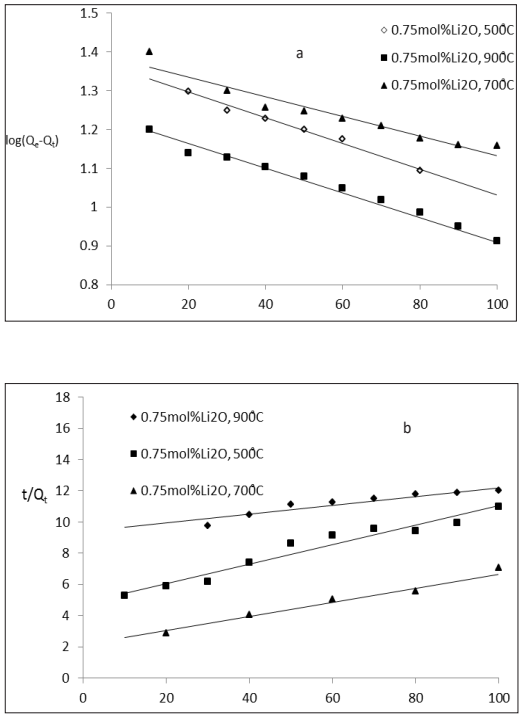

Fig. 10- Pseudo-first-order kinetics (a), and second-order kinetics (b) for Congo-Red dye adsorption onto 0.75 mol% Li_2O samples calcined at different temperatures (dye concentration = 50 ppm) at 35 ºC.

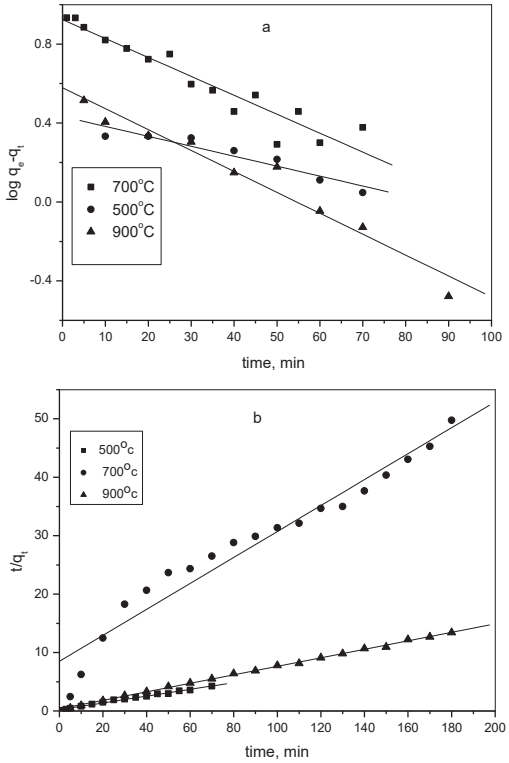

Fig. 11- Pseudo-first-order kinetics (a), and second-order kinetics (b) for Remazole-Red dye adsorption onto CuO-Fe_2O_3/ cordierite treated with 0.75% Li_2O samples and calcined at different temperatures (dye concentration = 50 ppm) at 35 ºC.

Table 5- Kinetic model constants and correlation coefficients for dyes adsorption on doped samples (C_0 = 34.83 mg.L^{-1}).

sample	Calc. Temp. ^{0}C	dye	$q_{e,}^{exp}$ (mg/g)	Pseudo first order model			Pseudo second order model		
				$q_{e,}^{cal}$ (mg/g)	k_1 (min^{-1})	R^2	$q_{e,}^{cal}$ (mg/g)	k_2 g/mg.min	R^2
CuO – Fe_2O_3 /cordierite +0.75% Li_2O	500	RR	3.8	1.542	0.0115	0.9008	4.5025	0.00834	0.950
	700		18.9	2.519	0.02421	0.9088	19.1210	0.20068	0.995
	900		13.4	1.742	0.01211	0.9543	13.7363	0.007305	0.999
CuO – Fe_2O_3/cordierite +3 mol% Li_2O	500	RR	4.8113	1.0102	0.01566	0.7738	6.1270	0.007681	0.994
	700		13.965	1.5683	0.02346	0.6537	14.7088	0.01165	0.990
	900		1.1735	1.0816	0.00369	0.6074	1.16038	0.004001	0.989
CuO – Fe_2O_3 /cordierite +0.75% Li_2O	500	CR	23.50	3.9298	0.0033	0.8454	23.04	0.000371	0.995
	700		26.89	4.6838	0.0064	0.9856	27.3224	0.000528	0.989
	900		16.54	3.8523	0.0052	0.7925	17.223	0.00047	0.979

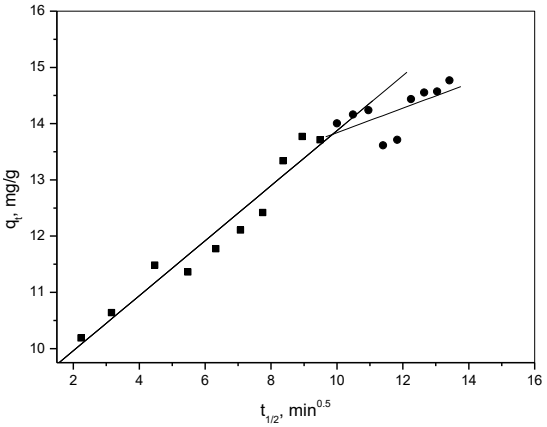

Fig. 12- intra-particle diffusion plot for Remazole-Red adsorption on 0.75 mol% Li_2O, CuO-Fe_2O_3/cordierite nanomaterials calcined at 700 ºC.

constants for phases I and II, respectively) from the slope of linear plots were 0.4893, and 0.1752 (mg/$min^{½}$ g). Although the plot for the dye was linear does not pass through the origin. So, the rate determing in the dyes adsorption process might be the boundary layer (film) diffusion.

3.5.5. Desorption and reuse results

Desorption and reuse is important in terms of costs and taking economic feasibility. The Congo-Red desorption was possible with NaOH as the dye was desorbed in 100 min. These findings confirm that electrostatic interactions are involved in the dye adsorption. The 0.75 mol% Li_2O nano-samples reuse was possible three times for Congo-Red maintaining no change in adsorption capacity (figure not given). Finally, it can be concluded that 0.75% Li_2O-doped material is an efficient adsorbent toward Congo-Red dye removing whose nature does not change even if it is used for three times.

3.6. The Catalytic properties of the solid in decomposition of H_2O_2

The decomposition of H_2O_2 has been widely studied for redox efficiency of homogeneous and heterogeneous catalysts [47]. The effect of insertion of Li_2O (0.75- 3 mole %) into CuO-Fe_2O_3/cordierite then heating at 500–900 ºC on the catalytic activity was investigated at 25 ºC as shown in Figs. 13 and 14. A straight line was obtained upon plotting ln a/a-x against the time intervals t, where (a) is the initial concentration of H_2O_2 and (a-x) is its concentration at time t. The reaction rate constant (k, min^{-1}) was determined from the slopes of (d ln a/a-x/dt) plots for the reaction conducted at a room temperature over a given catalyst.

Examination of results obtained show: (i) the reaction is good agreements with first-order kinetics. (ii) Treating CuO-Fe_2O_3/cordierite solid with Li_2O from 0.75 to 1.5 mol% led to increasing the catalytic activity of the computed k values for the catalytic reaction occurred at 25°C ($k_{25°C}$) over solids calcined at 700°C, which measured 1.8, 15.2, 8.1, 1.9 min^{-1} g^{-1}, for un-doped , 0.75, 1.5 and 3 mol% Li_2O, respectively. So, the increase is more pronounced in the catalytic activity due to 0.75 mol% Li_2O reached 700 %. This result may be related to the lowest particle size and the highest surface area of this sample, which also produced a large number of electrons donating active sites

for H_2O_2 decomposition (see Table 1). (iii) On the other hand, Further increase in Li_2O content to (3 mol%) decreases the S_{BET} values (table 1), which caused decreasing in the $k_{25°C}$ values attained 12.5, 90.9, and 44% for samples calcined at 500, 700, and 900 °C, respectively (figure not shown). (iv) The catalytic activity of the solids increases with increasing the temperature from 500 to 700 °C but further increase in the calcination temperature to 900 °C leads to decreasing the catalytic activity of H_2O_2 decomposition. (v) The investigated CuO-Fe_2O_3/cordierite system is active as oxidation-reduction catalyst.

The increase in the catalytic activity of treated solid samples with Li_2O (0.75 mol%) calcined at 700°C might be related to increasing the active sites concentration shared in the catalytic reaction by decreasing the crystallite size of CuO and $CuFe_2O_4$ phases (c.f. XRD section), also the presence of Li_2O as alkali. In fact, XRD data revealed that Li_2O of mixed oxides heated at 700 °C led a decrease in the intensity of diffraction lines of copper oxide indicating a high degree of dispersion of his oxide or a high surface concentration of active oxide. Increasing the catalytic activity by increasing the heating temperature from 500 to 700 °C has been attributed to an enhanced formation of $CuFe_2O_4$ phase which act as new active sites, beside increasing the S_{BET} as shown in Table 1, as mentioned previously, and decreasing the crystal size of CuO. Decreasing the catalytic activity of doped solids > 1.5 mol % Li_2O might be due to the decreasing hindrance of grain growth of CuO and small amount of Li_2O dissolves in cordierite matrix. These effects give big crystallites of CuO (c.f. XRD section). On the other hand, increasing the temperature from 500 to 900 °C led to decreasing the catalytic activity of the solid. The big decrease in the specific surface area might be the reason of the changes in the catalytic activities of different solids (c.f. Table 1).

The oxidation state of surface oxide catalysts is the most important factor influencing their activity [48]. Increasing of H_2O_2 catalytic decomposition by added metal oxide to cordierite samples might be due to the creation of active sites. The obtained results showed that the concentration of the catalytically active sites participate in chemisorption and catalysis of H_2O_2 increasing by doping process.

To inspect the permanence of the most active catalyst (0.75% Li_2O-doped solid (700 °C) was reused in four consecutive H_2O_2 decomposition runs at room conditiion (figure not given). The solid was filtered, washed, and dried, after each run, then reused for H_2O_2 decomposition. It was manifest that the catalytic efficiency doesn't alter even after four consecutive runs. This obviously imitates that the (0.75% Li_2O-doped solid has high stability and catalytic efficiency for H_2O_2 decomposition.

4. Conclusion

Photocatalytic activities of samples of CuO-Fe_2O_3/cordierite untreated and treated with Li_2O calcined at 700 °C on the degradation of some organic compounds were evaluated under UV-irradiation. Adsorptions of textile dyes (Remazole-Red and/or Congo-Red) from aqueous solution have been examined. The effect of contact time of

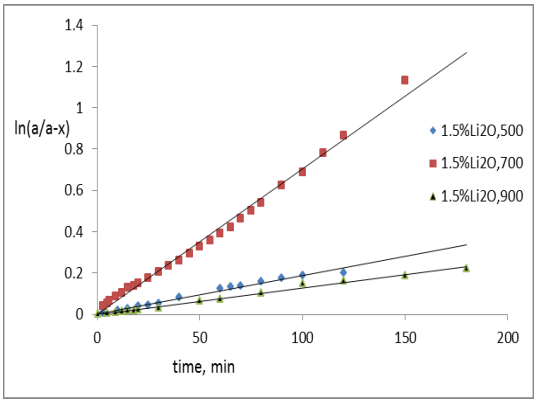

Fig. 13- First order plots for catalytic decomposition of H_2O_2, over (1.5 mol%) Li_2O treated solids calcined at different calcination temperature.

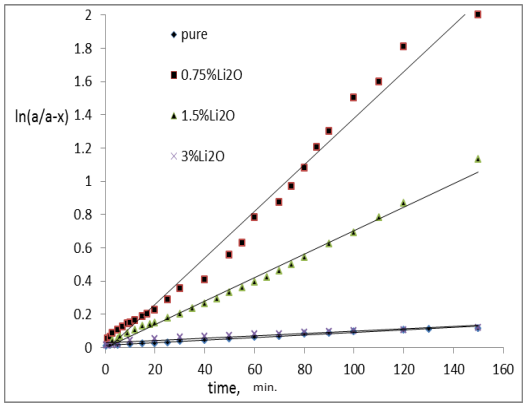

Fig. 14- First order plots for catalytic decomposition of H_2O_2, over untreated and treated samples solids calcined at 700°C.

attack with dye was considered. The results showed that Li_2O-treatment increase the photocatalytic degradation related to the amount of lithium introduced in the samples and the formation of single oxide phases. At low lithium percent (0.75 mol%) high photocatalytic activities had been procured that recorded degradation of 94% of the pollutant. Also, the obtained adsorption data showed that the adsorption increased gradually and the dye removal percentage improved with time. This might be attributed to vacant adsorption site on adsorbent material occupied by dyes deposited. The adsorption kinetics and isotherms showed that the sorption processes were better fitted by followed pseudo- second-order kinetics and the rate determing step in the process of Remazol-Red RB-133 dye adsorption was the boundary layer (film) diffusion. It can be concluded that CuO-Fe_2O_3/cordierite treated with 0.75% Li_2O are efficient adsorbent in Congo-Red or Remazole-Red dye removing whose nature does not change even if it is used for three times. The catalytic activity of different solids toward H_2O_2 decomposition was studied.The results showed that the concentration of the catalytically active sites participate in chemisorption and catalysis of H_2O_2 increasing by increasing of treatment percent. However, 0.75% Li_2O-doped solid was the highest stable and catalytic efficiency for H_2O_2 decomposition.

5. Acknowledgment

The study was supported by SABIC (SR-S-14-22), in the Deanship of scientific research, Qassim University

References

1. Yang W, Wu D, Fu R. Effect of surface chemistry on the adsorption of basic dyes on carbon aerogels. Colloids and Surfaces A: Physicochemical and Engineering Aspects. 2008;312(2-3):118-24.
2. Sismanoglu T, Kismir Y, Karakus S. Single and binary adsorption of reactive dyes from aqueous solutions onto clinoptilolite. Journal of Hazardous Materials. 2010;184(1-3):164-9.
3. Cristóvão RO, Tavares APM, Ribeiro AS, Loureiro JM, Boaventura RAR, Macedo EA. Kinetic modelling and simulation of laccase catalyzed degradation of reactive textile dyes. Bioresource Technology. 2008;99(11):4768-74.
4. Kansal SK, Hassan Ali A, Kapoor S. Photocatalytic decolorization of biebrich scarlet dye in aqueous phase using different nanophotocatalysts. Desalination. 2010;259(1-3):147-55.
5. Gök Ö, Özcan AS, Özcan A. Adsorption behavior of a textile dye of Reactive Blue 19 from aqueous solutions onto modified bentonite. Applied Surface Science. 2010;256(17):5439-43.
6. Toor M, Jin B. Adsorption characteristics, isotherm, kinetics, and diffusion of modified natural bentonite for removing diazo dye. Chemical Engineering Journal. 2012;187:79-88.
7. Cardoso NF, Pinto RB, Lima EC, Calvete T, Amavisca CV, Royer B, et al. Removal of remazol black B textile dye from aqueous solution by adsorption. Desalination. 2011;269(1-3):92-103.
8. Kara S, Aydiner C, Demirbas E, Kobya M, Dizge N. Modeling the effects of adsorbent dose and particle size on the adsorption of reactive textile dyes by fly ash. Desalination. 2007;212(1-3):282-93.
9. Badawy AA, Ibrahim SM, Essawy HA. Enhancing the Textile Dye Removal from Aqueous Solution Using Cobalt Ferrite Nanoparticles Prepared in Presence of Fulvic Acid. Journal of Inorganic and Organometallic Polymers and Materials. 2019.
10. Halim AA, Aziz HA, Johari MAM, Ariffin KS. Comparison study of ammonia and COD adsorption on zeolite, activated carbon and composite materials in landfill leachate treatment. Desalination. 2010;262(1-3):31-5.
11. Zhou J, Yang S, Yu J. Facile fabrication of mesoporous MgO microspheres and their enhanced adsorption performance for phosphate from aqueous solutions. Colloids and Surfaces A: Physicochemical and Engineering Aspects. 2011;379(1-3):102-8.
12. Meshkani F, Rezaei M. Facile synthesis of nanocrystalline magnesium oxide with high surface area. Powder Technology. 2009;196(1):85-8.
13. Mahato TH, Prasad GK, Singh B, Acharya J, Srivastava AR, Vijayaraghavan R. Nanocrystalline zinc oxide for the decontamination of sarin. Journal of Hazardous Materials. 2009;165(1-3):928-32.
14. Yang Y, Gao N, Chu W, Zhang Y, Ma Y. Adsorption of perchlorate from aqueous solution by the calcination product of Mg/(Al–Fe) hydrotalcite-like compounds. Journal of Hazardous Materials. 2012;209-210:318-25.
15. Zhang J, Li Y, Zhou J, Chen D, Qian G. Chromium (VI) and zinc (II) waste water co-treatment by forming layered double hydroxides: Mechanism discussion via two different processes and application in real plating water. Journal of Hazardous Materials. 2012;205-206:111-7.
16. Extremera R, Pavlovic I, Pérez MR, Barriga C. Removal of acid orange 10 by calcined Mg/Al layered double hydroxides from water and recovery of the adsorbed dye. Chemical Engineering Journal. 2012;213:392-400.
17. Liu X, Shen K, Wang Y, Wang Y, Guo Y, Guo Y, et al. Preparation and catalytic properties of Pt supported Fe-Cr mixed oxide catalysts in the aqueous-phase reforming of ethylene glycol. Catalysis Communications. 2008;9(14):2316-8.
18. Minicò S, Scirè S, Crisafulli C, Maggiore R, Galvagno S. Catalytic combustion of volatile organic compounds on gold/iron oxide catalysts. Applied Catalysis B: Environmental. 2000;28(3-4):245-51.
19. Trimm DL. Materials selection and design of high temperature catalytic combustion units. Catalysis Today. 1995;26(3-4):231-8.
20. Zhang W, Li S, Bao H, Zhao H, Ding Y. Study on the reaction process and mechanism of the system of cordierite with zirconia. Ceramics International. 2019;45(4):5066-71.
21. Tang W, Wang S, Xiao W, Du S, Lu X, Hoang S, et al. Pre-surface leached cordierite honeycombs for MnxCo3-xO4 nano-sheet array integration with enhanced hydrocarbons combustion. Catalysis Today. 2019;320:196-203.
22. Nascimento LF, Lima JF, de Sousa Filho PC, Serra OA. Effect of lanthanum loading on nanosized CeO2-ZnO solid catalysts

supported on cordierite for diesel soot oxidation. Journal of Environmental Sciences. 2018;73:58-68.
23. Ghanem AF, Badawy AA, Mohram ME, Abdelrehim MH. Enhancement the Photocatalytic and Biological Activity of Nano-sized ZnO Using Hyperbranched Polyester. Journal of Inorganic and Organometallic Polymers and Materials. 2019;29(3):928-38.
24. Ghanem AF, Badawy AA, Ismail N, Rayn Tian Z, Abdel Rehim MH, Rabia A. Photocatalytic activity of hyperbranched polyester/TiO2 nanocomposites. Applied Catalysis A: General. 2014;472:191-7.
25. Badawy A, Ibrahim S. Photocatalytic and Physicochemical Properties of Pure and Variously CeO2-doped CuO-Fe2O3/Cordierite System. International Research Journal of Pure and Applied Chemistry. 2017;14(3):1-8.
26. Abdel Rehim M, Badawy A. Nanocomposites for Abatement of Water Pollution. Nanocomposites for Pollution Control: Pan Stanford; 2018. p. 81-106.
27. Abdel Rehim MH, El-Samahy MA, Badawy AA, Mohram ME. Photocatalytic activity and antimicrobial properties of paper sheets modified with TiO2/Sodium alginate nanocomposites. Carbohydrate Polymers. 2016;148:194-9.
28. Cullity, B.D., Publishing Cos, 2nd ed., Addison-Wesley, Reading, MA, 1978, pp.102.
29. Robens E. Adsorption by powders and porous solids. F. Rouquerol, J. Rouquerol, K. Sing, Academic Press, San Diego 1999, ISBN: 0-12-598920-2, 467 S. £79.95. Vakuum in Forschung und Praxis. 1999;11(3):191-.
30. Chen Y, Stathatos E, Dionysiou DD. Sol–gel modified TiO2 powder films for high performance dye-sensitized solar cells. Journal of Photochemistry and Photobiology A: Chemistry. 2009;203(2-3):192-8.
31. Langmuir I. THE ADSORPTION OF GASES ON PLANE SURFACES OF GLASS, MICA AND PLATINUM. Journal of the American Chemical Society. 1918;40(9):1361-403.
32. Freundlich, H.M.F., Over the adsorption in solution. J. Phys. Chem 1906, 57(385471):1100-1107.
33. White E. The chemistry of imperfect crystals By F. A. Kr ger. Pp. xvi + 1039. North-Holland Publishing Co., Amsterdam. 1964. E11 net. Endeavour. 1964;23(90):168.
34. Zhu P, Wang LY, Hong D, Zhou M. A study of cordierite ceramics synthesis from serpentine tailing and kaolin tailing. Science of Sintering. 2012;44(2):129-34.
35. Wang Y, Tian D, Chu W, Li M, Lu X. Nanoscaled magnetic CuFe2O4 as an activator of peroxymonosulfate for the degradation of antibiotics norfloxacin. Separation and Purification Technology. 2019;212:536-44.
36. AlSalka Y, Granone LI, Ramadan W, Hakki A, Dillert R, Bahnemann DW. Iron-based photocatalytic and photoelectrocatalytic nano-structures: Facts, perspectives, and expectations. Applied Catalysis B: Environmental. 2019;244:1065-95.
37. Mahmoud HR, Ibrahim SM, El-Molla SA. Textile dye removal from aqueous solutions using cheap MgO nanomaterials: Adsorption kinetics, isotherm studies and thermodynamics. Advanced Powder Technology. 2016;27(1):223-31.
38. Ibrahim SM, El-Molla SA. Textile dye removal from aqueous solutions using cheap MgO nanomaterials: Adsorption kinetics, isotherm studies and thermodynamics. Advanced Powder Technology. 2016;27(1):223-31.
39. Wei Z, Xing R, Zhang X, Liu S, Yu H, Li P. Facile Template-Free Fabrication of Hollow Nestlike α-Fe2O3 Nanostructures for Water Treatment. ACS Applied Materials & Interfaces. 2012;5(3):598-604.
40. Vimonses V, Lei S, Jin B, Chow CWK, Saint C. Kinetic study and equilibrium isotherm analysis of Congo Red adsorption by clay materials. Chemical Engineering Journal. 2009;148(2-3):354-64.
41. Morais WA, de Almeida ALP, Pereira MR, Fonseca JLC. Equilibrium and kinetic analysis of methyl orange sorption on chitosan spheres. Carbohydrate Research. 2008;343(14):2489-93.
42. Guibal E, McCarrick P, Tobin JM. Comparison of the Sorption of Anionic Dyes on Activated Carbon and Chitosan Derivatives from Dilute Solutions. Separation Science and Technology. 2003;38(12-13):3049-73.
43. Feng T, Zhang F, Wang J, Huang Z. Notice of Retraction: Adsorption of Congo Red by Cross-Linked Chitosan Film. 2011 5th International Conference on Bioinformatics and Biomedical Engineering; 2011/05: IEEE; 2011.
44. Cestari AR, Vieira EFS, Tavares AMG, Bruns RE. The removal of the indigo carmine dye from aqueous solutions using cross-linked chitosan—Evaluation of adsorption thermodynamics using a full factorial design. Journal of Hazardous Materials. 2008;153(1-2):566-74.
45. Ho Y-S. Absorption of heavy metals from waste streams by peat: University of Birmingham; 1995.
46. Bharathi KS, Ramesh ST. Removal of dyes using agricultural waste as low-cost adsorbents: a review. Applied Water Science. 2013;3(4):773-90.
47. Ibrahim SM, Badawy AA, El-Shobaky GA, Mohamed HA. Structural, surface and catalytic properties of pure and ZrO2-doped nanosized cobalt-manganese mixed oxides. The Canadian Journal of Chemical Engineering. 2013;92(4):676-84.
48. Badawy AA, Ibrahim SM. The influence of La2O3-doping on structural, surface and catalytic properties of nano-sized cobalt–manganese mixed oxides. International Journal of Industrial Chemistry. 2016;7(3):287-96.